Hindawi
Shock and Vibration
Volume 2017, Article ID 3675470, 12 pages
https://doi.org/10.1155/2017/3675470

Research Article

Arc-Surfaced Frictional Damper for Vibration Control in Container Crane

Gongxian Wang, Yang-Yang Wang, Jianming Yuan, Yi Yang, and Dong Wang

School of Logistics Engineering, Wuhan University of Technology, Wuhan 430063, China

Correspondence should be addressed to Jianming Yuan; whtu_yjm@163.com

Received 14 November 2016; Accepted 12 January 2017; Published 9 February 2017

Academic Editor: Marcello Vanali

In this paper, a new arc-surfaced frictional damper (AFD) is proposed and its hysteretic behavior is experimentally studied. Then the device is applied to container crane based on a seesaw mechanism. The major advantage of the seesaw damping system is that the long tension cables can be utilized as bracing between the seesaw member and the portal legs to avoid compression and buckling of the cables. A simplified trilinear force-displacement model on the basis of experimental results is adopted to represent the hysteretic behavior of AFD. After that, seismic responses of container crane with and without dampers to four earthquakes are studied using nonlinear dynamic time-history analysis. Besides this system, a diagonal-brace-AFD system is studied for comparison. A method based on the displacement and energy dissipation ratio is proposed to find the optimum slip force for seesaw damping system. Performance of AFD control system is assessed though various parameters including displacement and maximum portal frame drift angle. Results prove a feasible application of AFD control system to absorb large amounts of seismic energy and significantly reduce the structural responses.

1. Introduction

Frictional damper has been proved to be an efficient approach to improve the seismic performance of the structures since the device can dissipate lager amounts of seismic energy to prevent structural collapse during earthquake ground motions. For the last few decades, several frictional dampers have been developed for structural application.

Rotational friction damper (RFD) was introduced by Mualla and Belev [1]. Experimental and numerical studies were conducted on a single story frame equipped with RFD. Liao et al. [2] carried out a shake table test on a three-story steel frame with RFD. The results proved the effectiveness of RFD in reducing the seismic responses. Kim et al. [3] utilized RFDs to improve progressive collapse-resisting capacity and mitigate the vibration of concrete moment frame. Sanati et al. [4] updated RFD with viscoelastic pads (RFVD). Experimental results conducted on a scaled steel frame with RFVD indicated a better performance of reducing seismic responses compared to the RFD. Mirzabagheri et al. [5] conducted a test on RFDs with different units, observed that more energy was dissipated by increasing number of units, and then proposed an equivalent method to evaluate the performance of RFDs. Cylindrical friction damper (CFD) was proposed by Mirtaheri et al. [6], both experimental and numerical research were carried out to evaluate hysteretic behavior of the damper. Time-history analyses were conducted on a frame with CFDs and results show that the device is capable of improving seismic performance. Monir and Zeynali [7] proposed a modified friction damper and primary experiments were carried out on a SDOF steel frame equipped with the damper. The experimental and numerical analyses revealed that the friction damper can reduce the displacement and story drifts.

Container crane is one of the most important types of equipment in the port. In the recent years, large cranes are needed more than ever. Consequently, modern container is more vulnerable to earthquakes. A few works have been done in the field of seismic control of container cranes. Sagirli et al. [8] studied self-tuning fuzzy logic controllers to suppress structural vibrations of a crane under the earthquake excitation and numerical studies proved that the control strategy is a feasible method. Azeloglu et al. [9, 10] developed the fuzzy PID type controller and a linear matrix

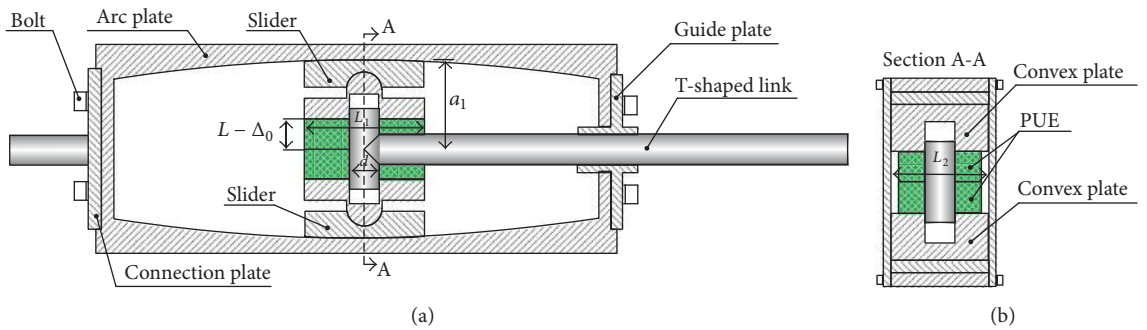

Figure 1: Schematic illustration of AFD: (a) longitudinal section and (b) cross section.

inequality based mixed H_2/H_∞ state-feedback controller to reduce seismic response of a crane. They concluded that the proposed controllers have great potential in vibration control for container cranes.

Gong-Xian et al. [11] proposed a seismic control method for a container crane based on the principle of energy dissipation. Four viscous dampers supported by the braces were installed in the structure. The equivalent viscous damping and the stiffness were deduced and the optimization method based on displacement and energy dissipation ratio was proposed. It was concluded that the proposed method could effectively dissipate seismic energy and control the seismic responses.

In spite of efforts to improve seismic response of container crane, there is still a lack of study on the use of frictional dampers to reduce the seismic responses and seismic analyses of the crane with dampers. Their implementation is still limited due to the unavailability of reliable technologies and high costs. This paper proposes a novel AFD which can provide variable frictional force. The hysteretic behavior of the device is then experimentally studied. After that, a simplified trilinear force-displacement model for AFD based on the experimental results is suggested to be utilized in seismic response analyses. The vibration control system based on a seesaw mechanism using AFDs is introduced. Besides this, the diagonal-brace-AFD system is studied for comparison. The optimization method for the slip load of AFDs is proposed. Analyses on seismic responses are conducted for the cranes with AFDs and compared to the bare structure.

2. Arc-Surfaced Frictional Damper (AFD)

The main parts of AFD are arc plate, slider, convex plate, Polyurethane Elastomer (PUE), and T-shaped link. A schematic illustrate of the proposed AFD is presented in Figure 1. The arc plate is designed to fit with the slider, and their contact surfaces are circular and have same radius. Two blocks of PUE are shrink fitted middle two convex plates which contact with the slider through the surface of the cylinder. Consequently, the sliders and the arc plates are closely banded with each other with the normal force provided by PUE. Two sliders and two blocks of PUE are installed onto the T-shaped link which can make them move together. Furthermore, the distance of the arc plates is getting smaller when two sliders are moving close to the end of AFD. During this process, the slider will rotate at a certain degree, which makes the slider and the plate well matched. Since the distance of the two plates is variable, the damping force will change with the moving of sliders during the motion.

Table 1: Specification of test cases.

Test case	Δ_0 (mm)	L_1 (mm)	L_2 (mm)	L (mm)	Stroke (mm)	Frequency of loading (Hz)
Case A	3	80	65	23	±60	0.05
Case B	5	80	65	25	±60	0.05
Case C	7	80	65	27	±60	0.05

Δ_0 = precompression of PUE, L_1 = width of PUE, L_2 = length of PUE, and L = thickness of PUE.

3. Experimental Study

3.1. Experimental Setup. The damper consists of three kinds of materials, which are defined by Chinese Industrial Standards. The arc plate with the width of 65 mm and radius of 1000 mm was made from 45 steel with a 354 MPa yield stress and 598 MPa ultimate strength. The sliders with the radius of 1000 mm were made from brass, as shown in Figure 2(a).

To obtain energy dissipation capacity and hysteric behavior of AFD, tests were carried out on the universal machine with a capacity of 50 kN. The specifications are presented in Table 1. Figure 2(b) shows the test set up in which both the ends of AFD were installed in the load cells of the testing machine and the bottom load cell applied cyclic loading to the AFD with predetermined amplitudes. The data acquisition system was used to record the experimental data.

3.2. Experimental Results. The hysteretic behaviors of AFDs under cyclic loading with 0.05 Hz frequency are presented in Figure 3. As one could expect, the hysteretic curves with stable hysteresis loops are saddle-shaped. There is a sharp slope on the upper and bottom hysteretic curves. This was induced by the inertia force of the sliders. In the curves, a step appears with the slope crossing x-axis, the reason for this is that there is a gap between the load cell and fixture. As can be seen in Figure 3, the frictional force increases with the increasing

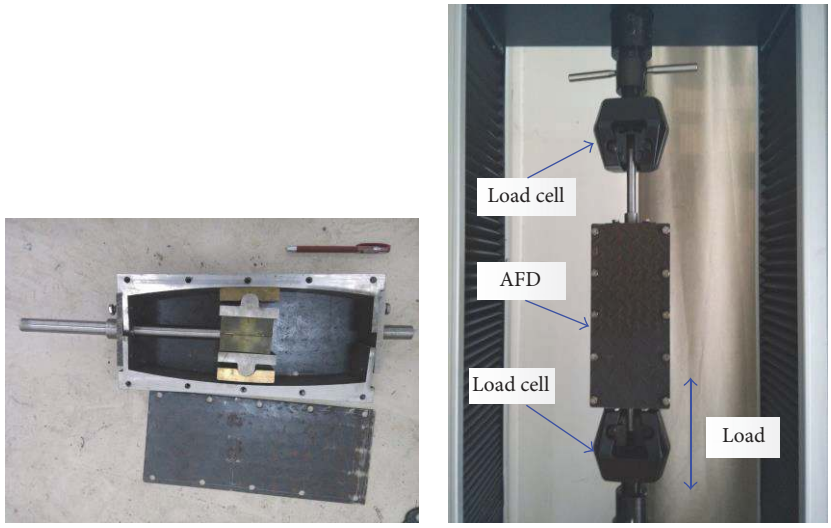

(a) (b)

Figure 2: Test setup: (a) main parts of AFD and (b) test frame.

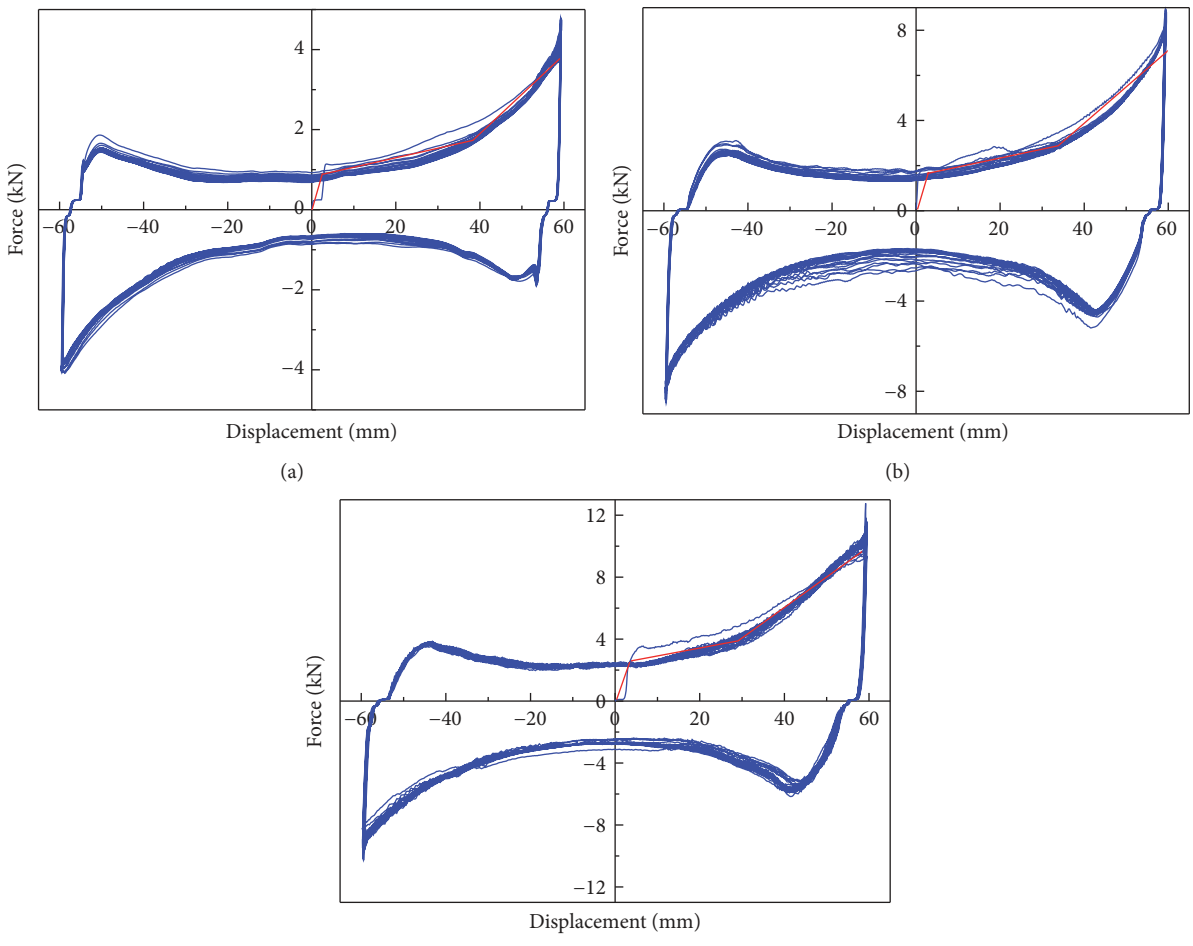

Figure 3: Hysteretic behavior of AFD: (a) Case A, (b) Case B, and (c) Case C.

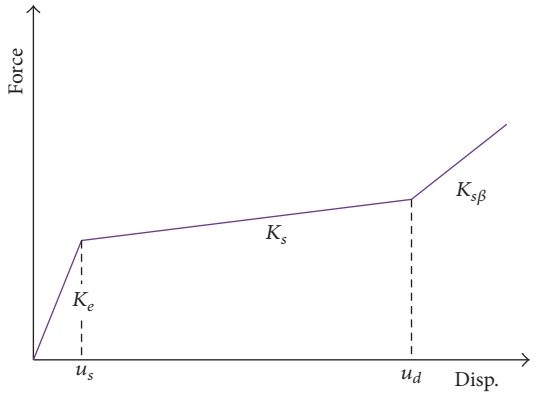

Figure 4: Simplified trilinear characteristic force-displacement for AFD.

displacement. This is caused by the distance between the two arc surfaces getting smaller so that the compression of PUE increases. So, the normal forces acting on the sliders increase, which results in the increasing frictional force. It is noted that the slip load crossing y-axis for case C is 2.395 kN, and the maximal one reaches 11.07 kN. This indicates that the device is capable of providing large damping force. For the limitation of test machine, it may be expected that AFD can demonstrate larger damping force with larger configuration.

4. Simplified Force-Displacement Model for AFD

To investigate the effectiveness of AFD in reducing seismic response of container crane, a simplified force-displacement model is very helpful and can be used to model AFD in some analysis software. For this purpose, the hysteretic behavior for AFD can be idealized by a trilinear model, as shown in Figure 4. The model is able to consider variable frictional force of AFD. In this figure, K_e, K_s, and $K_{s\beta}$ are, respectively, the initial lateral stiffness, the nonlinear stiffness, and the large deformation stiffness of AFD. The displacement (u_s, u_d) at which the stiffness changes to the nonlinear stiffness and the large deformation stiffness can be calculated, based on the results of experimental results.

Figure 3 shows the simplified trilinear force-displacement for AFD. It can be seen that the simplified model can work well as the essential characteristics of AFD.

5. Behavior of Container Crane with AFDs

The total system is composed of the original system and AFD vibration control system. The idealized force-displacement relationship of container crane with AFDs is illustrated in Figure 5. The overall stiffness of the bare structure includes the effect of stiffness reduction. K_b and $K_{b\alpha}$ are, respectively, the initial and the secondary stiffness of the bare structure. u_y is the yield displacement of the crane, at which the stiffness changes to the secondary stiffness.

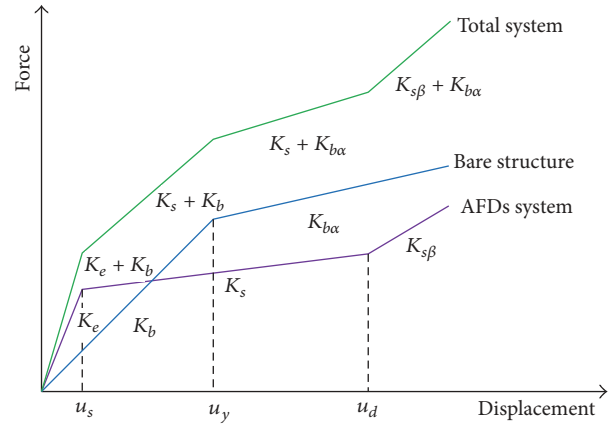

Figure 5: Load-displacement relationship of container crane with AFDs.

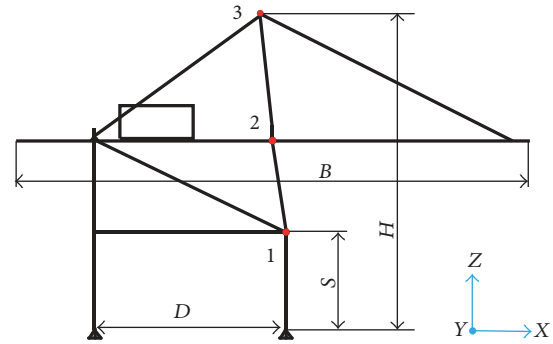

Figure 6: Container crane (bare structure).

Table 2: Container crane properties used in analysis.

Model	D (m)	S (m)	B (m)	H (m)	Material	Mass (t)
BS	30.5	14.5	49.7	30.5	A36	545

D = portal gage, S = portal height, B = beam length, and H = total height.

6. Seismic Responses of Container Crane with AFDs

6.1. Bare Structure. Container crane used for analyses is shown in Figure 6. The properties of the crane that is considered for analysis are shown in Table 2. Under working condition, the wheel mechanism is in the braking stage, the crane cannot move on the rail, and the wheel-rail connection can be negligible, so the portal legs are hinged on the ground. In this model, trolley, counterweight, and payload are considered as point masses lumped at the center of mass of the corresponding element.

6.2. Description of Analysis Models. In order to examine the effectiveness of AFD vibration control system, the program SAP2000 was used to analyze the responses of container crane equipped with AFDs. The crane is modeled using the beam element with plastic hinges at the member ends. Table 3 lists the material properties of A36 used in analysis.

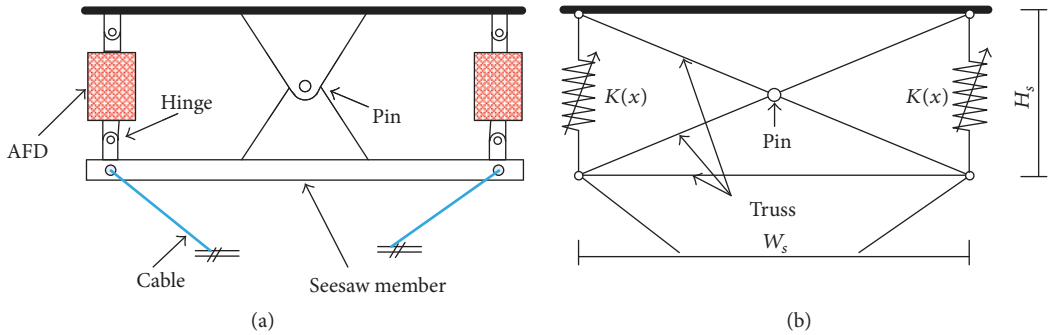

Figure 7: Model of vibration control system: (a) details of vibration control system and (b) analysis model.

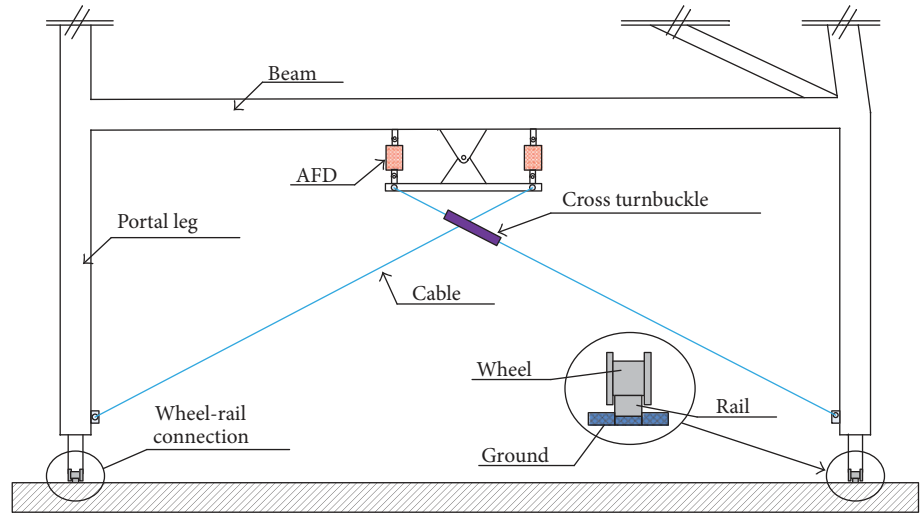

Figure 8: Container crane with AFDs.

Table 3: Material properties used in analysis.

Material	Modulus of elasticity (MPa)	Yield stress (MPa)	Poisson's ratio
A36	210×10^5	250	0.3

A damping ratio of 2% is considered for all mode shapes in the analysis.

Figure 7(a) depicts the details of vibration control system [12, 13] including a couple of AFDs, tension cables, and a pin-supported seesaw member. The analysis model is shown in Figure 7(b), in which the cables are modeled by the elastic spring element and some rigid truss members from both the seesaw member and the pin-support. The AFDs are modeled using Multilinear Plastic elements $K(x)$ with simplified hysteretic behavior depicted in Section 4.

Figure 8 presents the vibration control system installed in the crane. A couple of AFDs are connected to the beam and the seesaw member with the hinges. The long cables with cross turnbuckle are used in the mechanism to connect the seesaw member to the portal legs, on which the pretension force is applied to keep them from compression and buckling. Figure 9 illustrates the mechanism of the damping system. When a lateral load excites the crane, the portal legs tend to sway dramatically. The beam is inclined to move horizontally, which will resist the deformation of portal legs by the combination of the structure and fictional forces.

Three analysis models of container crane are established. Figure 10(a) presents the bare structure without damping system (Model BS), as depicted in Section 6.1. Others are structures equipped with AFD vibration control system, as presented in Figure 10(b and c). Figure 10(b) shows one case concerns the structure with the diagonal-brace-AFD system (Model DB), connecting the portal leg with the beam at the mid-span. The rods are modeled as rigid body. h represents the distance of the bottom point of each brace from the ground level, as shown in Table 4. By contrast, the structure with seesaw system (Model SS) has two damping devices on the beam, as shown in Figure 10(c).

6.3. Earthquake Ground Motion. A suit of four earthquake records of different peak ground acceleration (PGA) and domain periods is chosen for time-history analyses. The ground motions include the 1940 El Centro earthquake, the 1952 Taft earthquake, the 1994 Northridge earthquake, and

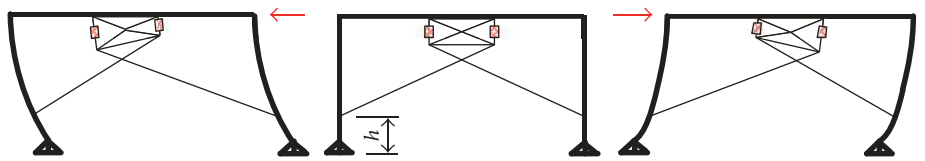

Figure 9: Mechanism of the control system with AFDs.

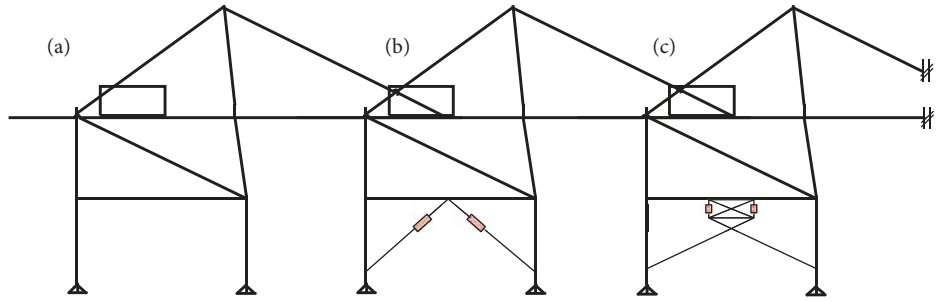

Figure 10: Analysis models: (a) Model BS, (b) Model DB, and (c) Model SS.

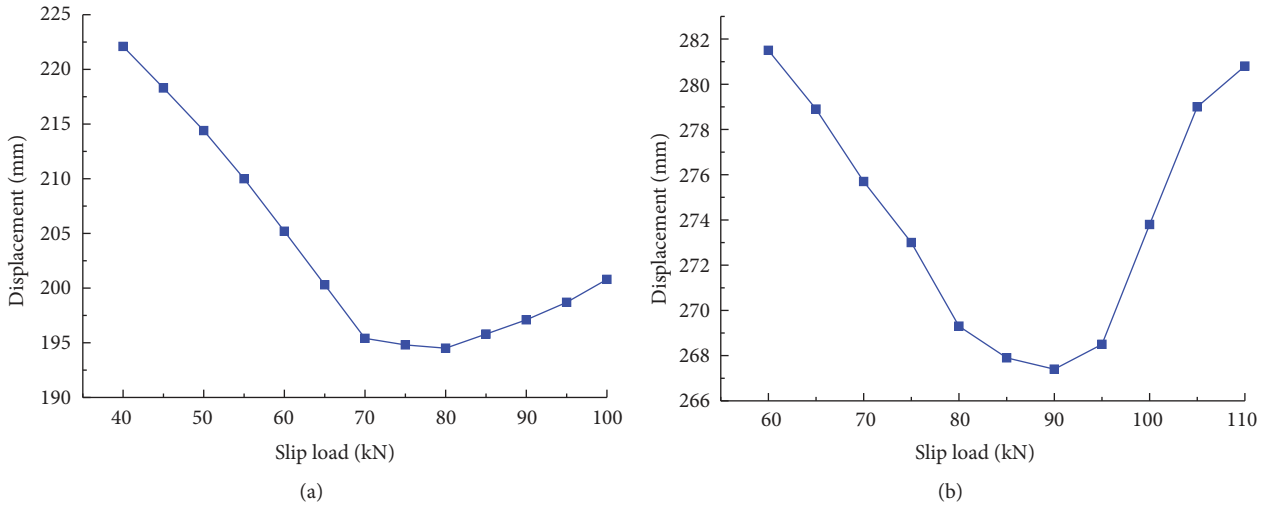

Figure 11: Maximum displacement at the top of the crane versus slip load: (a) PGA = 0.4 g and (b) PGA = 0.62 g.

the 1995 Kobe earthquake, as presented in Table 5. These records are scaled to produce the peak ground acceleration of 0.4 g and 0.62 g. According to the Chinese standards, the two values correspond to 7- and 8-degree earthquakes, respectively.

6.4. Optimum Slip Load. In order to dissipate the input energy as much as possible, some slip forces must be examined to find the optimum slip force. Subsequently, a parametric study based on the displacement and energy dissipation ratio is conducted until the minimum displacement at the top of container crane (point 3, see Figure 6) and the maximum energy dissipation ratio are reached.

Figure 11 presents the maximum displacement versus slip load for Model SS under the El Centro earthquake. As can be seen in Figure 11(a), the values of the slip load range from 40 kN to 100 kN, and results show that the maximum displacement at the top of the crane varies according to the slip load. In case where the slip load is equal to 80 kN for PGA = 0.4 g, the minimum displacement at the top of the crane is reached.

The normalized E_D/E_I ratio, in which E_D is the energy dissipated by AFDs and E_I is the input energy, is calculated

Table 4: Analysis parameters.

Model	k_B (kN/mm)	N	W_S (mm)	H_S (mm)	h (mm)
Model DB	∞	4	—	—	6096
Model SS	27	4	3600	1200	6096

k_B = rod stiffness, N = number of AFDs, W_S = width of seesaw, H_S = height of seesaw, and h = height of rod from ground.

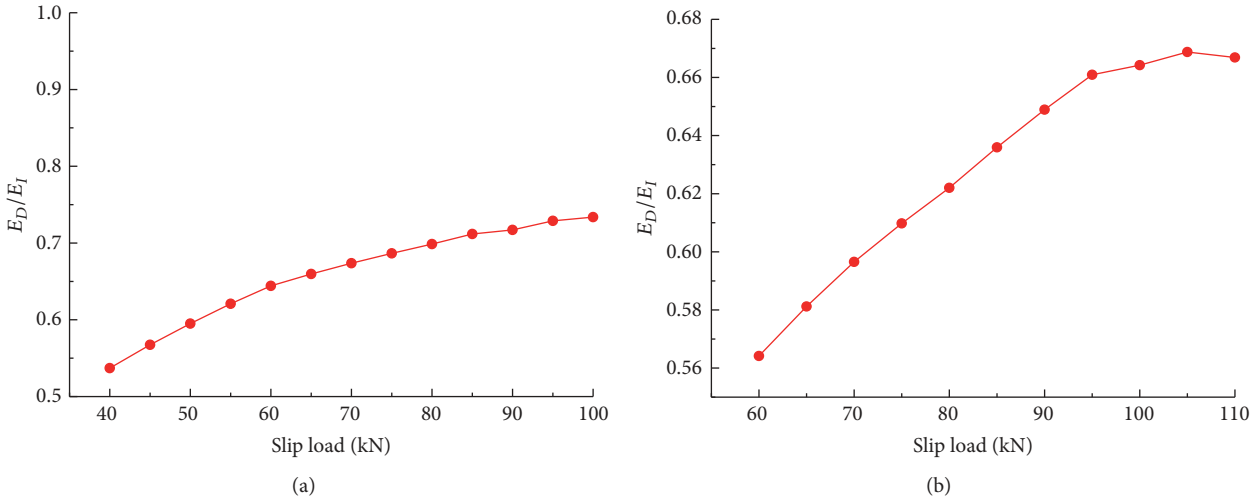

Figure 12: Energy dissipated by AFDs normalized by the input energy: (a) PGA = 0.4 g and (b) PGA = 0.62 g.

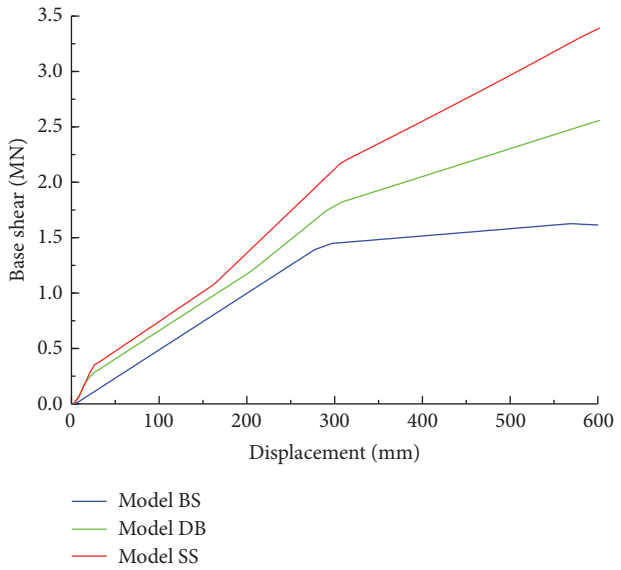

Figure 13: Nonlinear pushover curves.

Table 5: Earthquake ground motions.

Input motion	Year	PGA (g)	Domain period (s)	Duration (s)
El Centro NS	1940	0.44 0.62	1.462	30
Taft EW	1952	0.44 0.62	0.368	30
Northridge EW	1994	0.44 0.62	1.138	30
Kobe NS	1995	0.44 0.62	1.241	30

and shown in Figure 12. As shown in Figure 12(a), when the slip load ranges from 40 kN to 100 kN, the E_D/E_I ratio increases from 0.53 to 0.73. This indicates that the vibration control system using AFDs is capable of consuming more than half of the input energy. For cases when the slip load is larger than 80 kN, the slip load has little effect on the E_D/E_I ratio.

From the results presented in Figures 11 and 12, the optimum slip loads are 80 kN and 90 kN for PGA = 0.4 g and PGA = 0.62 g, respectively. They are used for the time-history response analyses in the following section.

6.5. Seismic Responses of Container Crane

6.5.1. Nonlinear Pushover Curves. Static pushover analyses are conducted on the bare structure and models with the optimum slip load whose value is 80 kN. The curves of base shear force versus the displacement at the top of the crane are plotted in Figure 13. As can be seen in this figure, introducing

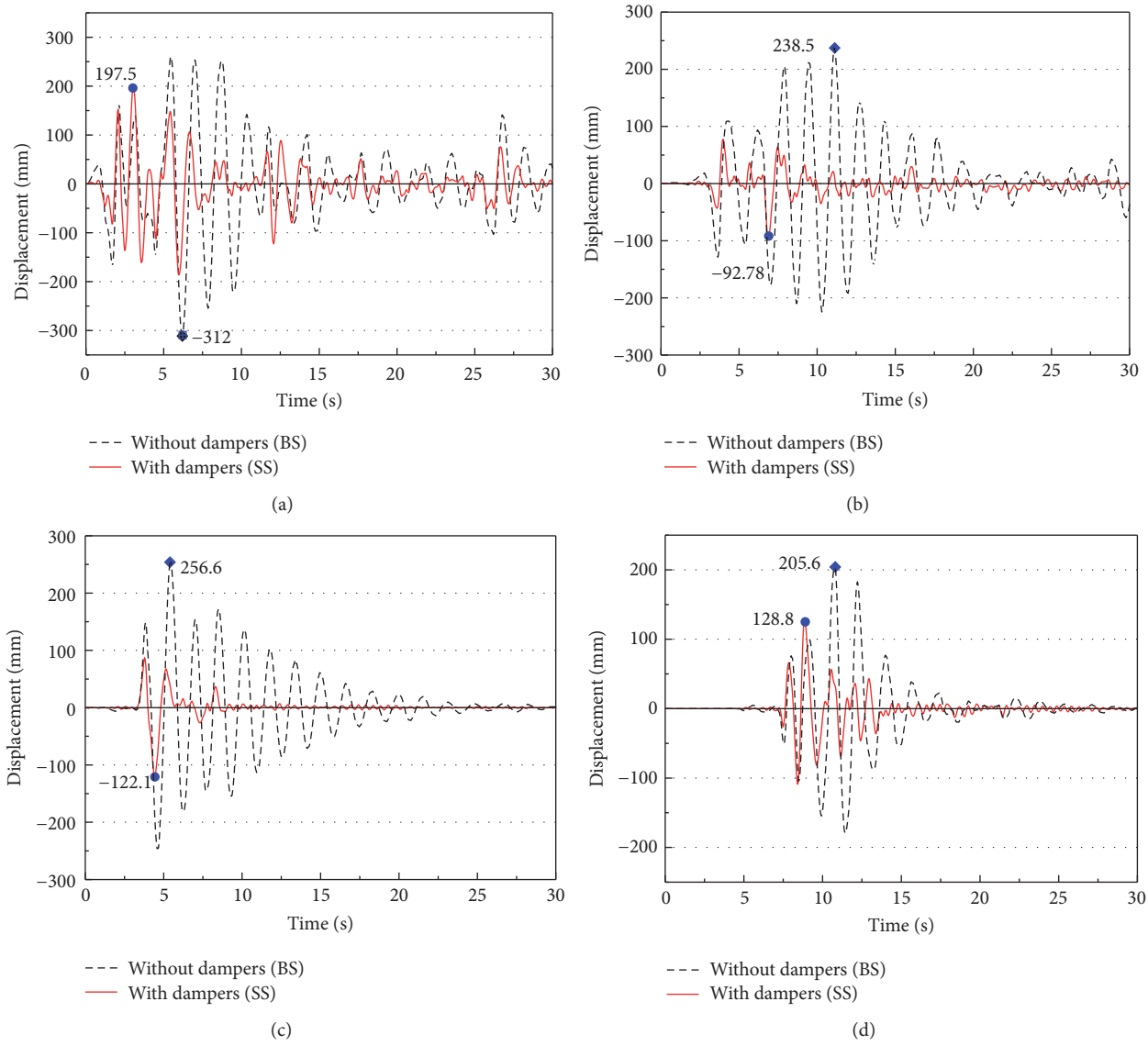

Figure 14: Time-history response of displacement at the top of the portal leg of Models BS and SS for PGA = 0.4 g: (a) El Centro, (b) Taft EW, (c) Northridge EW, and (d) Kobe NS.

AFDs to container crane alters the force-displacement relationship to a shape which is similar to that plotted in Figure 5. Both the stiffness and the strength of the entire system are changed by adding the vibration control systems. Seesaw damping system, as expected, has a better performance of enhancing strength than that of the diagonal brace control system.

6.5.2. Displacement Response. Figures 14 and 15, respectively, represent the comparative plots of seismic response of displacement at the top of Model BS and SS for PGA = 0.4 g and 0.62 g. These figures verify the effectiveness of the vibration control system in reducing the response of displacement. The maximum displacement at the top of the crane for PGA = 0.4 g and 0.62 g are marked with the value and bracketed in Table 6. The ratios of the attenuation with dampers to that without dampers are also presented, in which the maximum damping ratios for both seismic intensities can reach 61%. More than that, it demonstrates that the time-history of displacement reduction in Model SS is larger than the other.

6.5.3. Maximum Portal Frame Drift Angle Distribution. Figures 16 and 17, respectively, show the maximum portal frame drift angle distributions of different points (see Figure 6) for PGA = 0.4 g and 0.62 g. In all cases, the portal frame drift angle distributions were reduced by the vibration control system with AFDs. By contrast, the vibration control system with a seesaw mechanism can achieve a better result. So the seesaw vibration control system with AFDs is a feasible way to improve seismic response of container crane.

Table 6: Maximum displacement at the top of the structure.

Input motion	PGA (g)	Model	Without dampers (mm)	With dampers (mm)	Ratio
El Centro NS	0.44	Model DB	312	209.2	0.33
		Model SS		197.5	0.37
	0.62	Model DB	403.2	280.8	0.30
		Model SS		266.3	0.34
Taft EW	0.44	Model DB	238.5	107.2	0.55
		Model SS		92.78	0.61
	0.62	Model DB	308.1	137.8	0.55
		Model SS		118.7	0.61
Northridge EW	0.44	Model DB	256.6	161	0.37
		Model SS		122.1	0.52
	0.62	Model DB	331.7	218.6	0.34
		Model SS		171	0.48
Kobe NS	0.44	Model DB	205.6	154	0.25
		Model SS		128.8	0.37
	0.62	Model DB	265.7	226.7	0.15
		Model SS		172.7	0.35

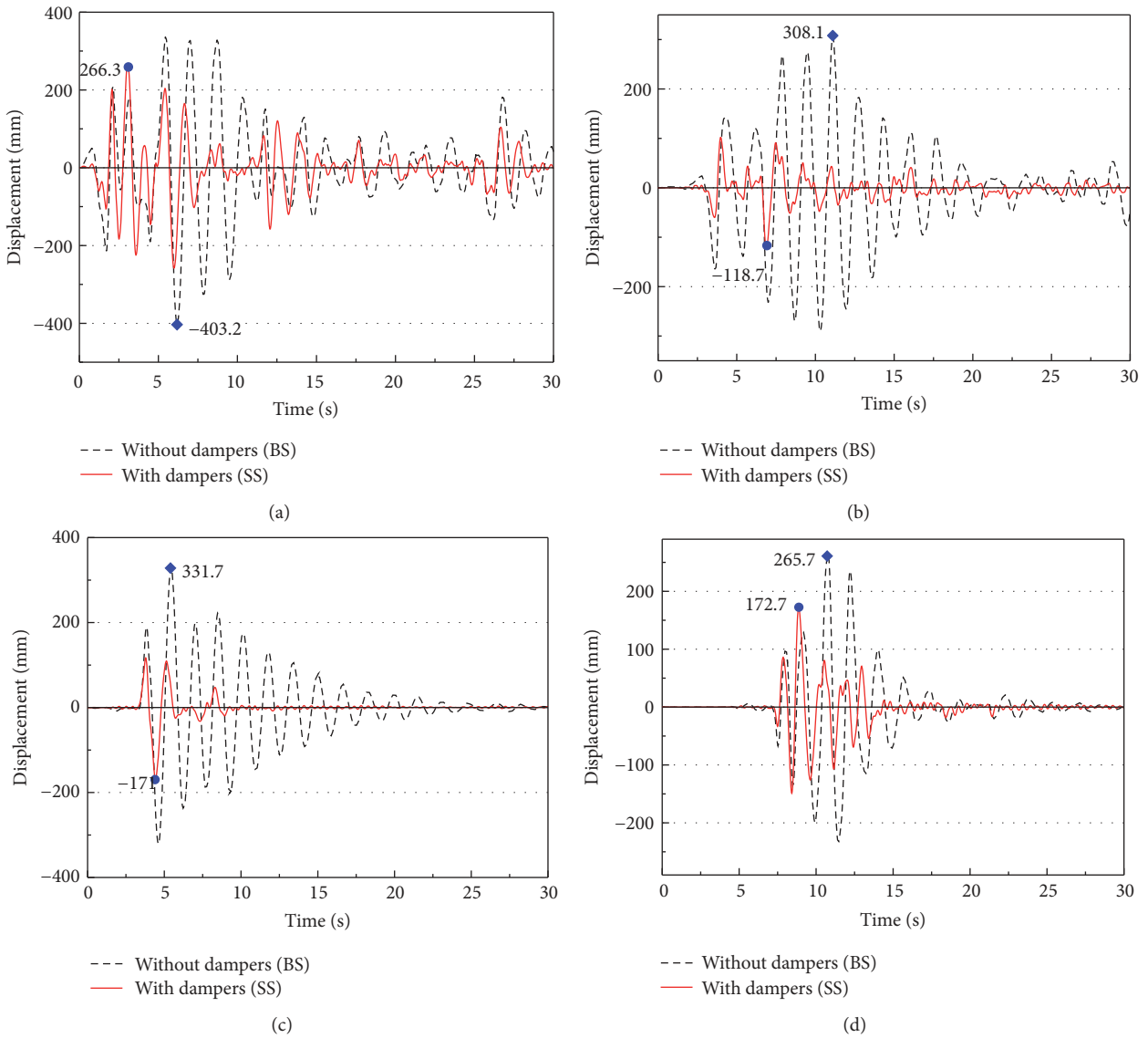

Figure 15: Time-history response of displacement at the top of the portal leg of Models BS and SS for PGA = 0.62 g: (a) El Centro, (b) Taft EW, (c) Northridge EW, and (d) Kobe NS.

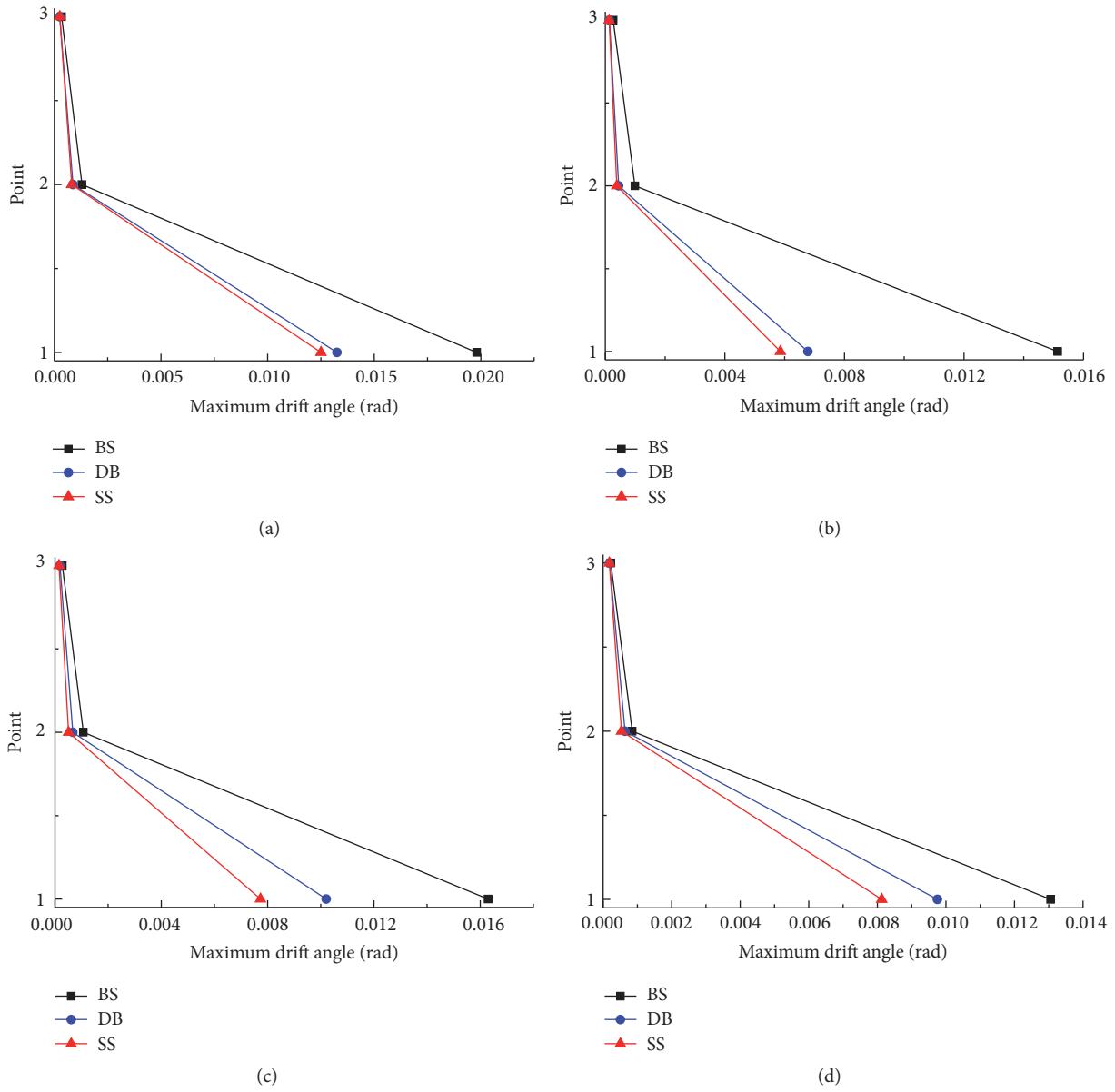

Figure 16: Maximum drift angle distribution for PGA = 0.4 g: (a) El Centro NS, (b) Taft EW, (c) Northridge EW, and (d) Kobe NS.

7. Conclusion

A new arc-surfaced frictional damper for seismic reduction of container crane was proposed and assessed experimentally. The variable frictional force and stable hysteretic loop are secured by the compression of PUE. A vibration control system using seesaw mechanism equipped with AFDs was introduced. First, a simplified trilinear force-displacement model of AFD was suggested based on the experimental results.

To investigate the effectiveness of this vibration control system, seismic response analyses were then carried out for a container crane with the system. The diagonal-brace-AFD system was also studied for comparison. Time-history responses of displacement, maximum portal frame drift angle were examined. Comparisons between seismic responses of bare structure and that equipped with damping system were conducted. The results show that the displacement is reduced by up to 61% both for PGA = 0.4 g and PGA = 0.62 g. The maximum drift angle is remarkably less compared to that of diagonal-brace-AFD system. The optimization method for the slip force on the basis of the displacement and the energy dissipation ratio is proposed.

The major advantage of the seesaw damping system is that the long tension cables can be utilized as bracing between the seesaw member and the portal legs to avoid compression and buckling of the cables. Seesaw vibration control system with AFDs is a feasible way to improve seismic response of container crane.

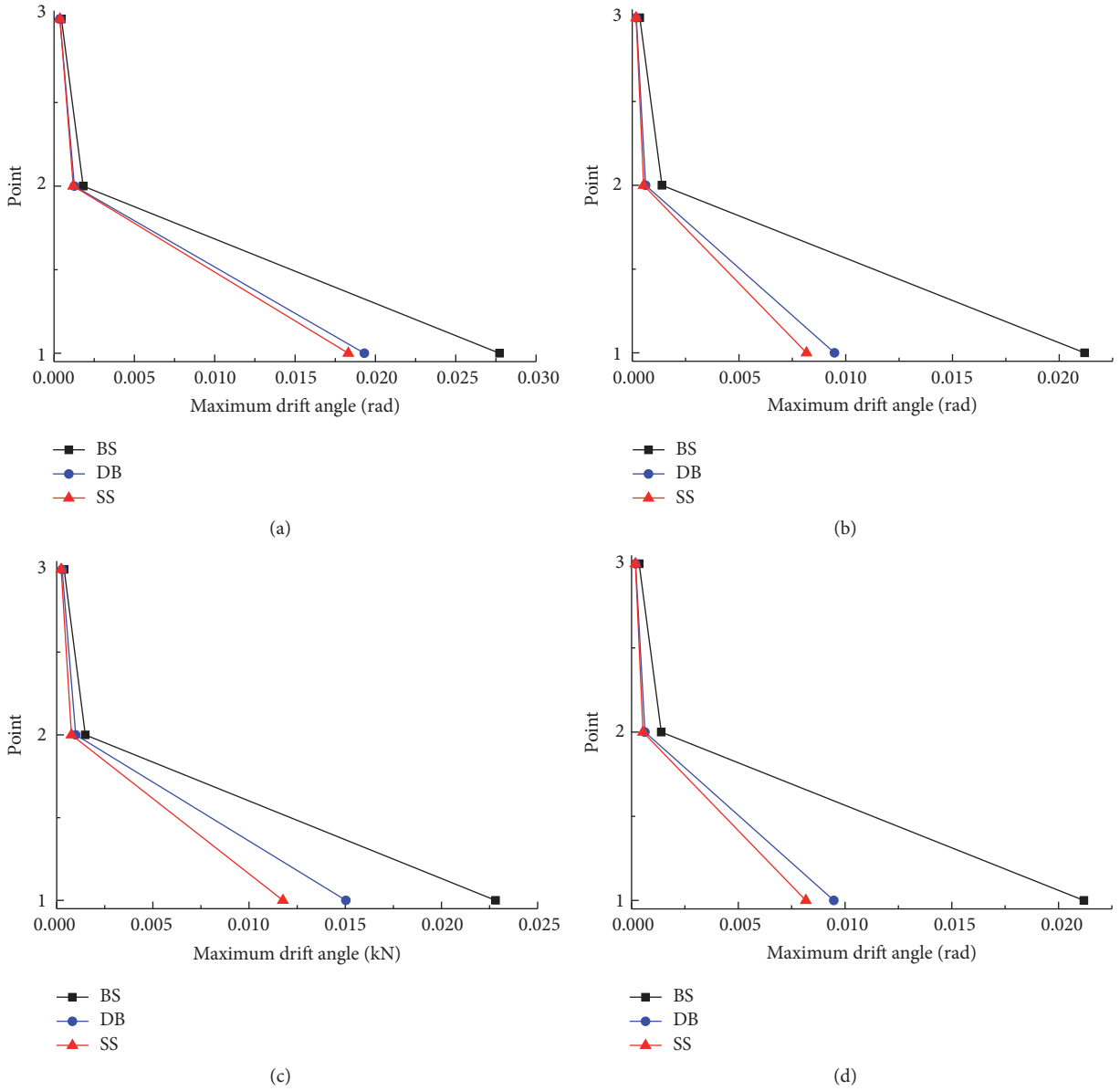

Figure 17: Maximum drift angle distribution for PGA = 0.62 g: (a) El Centro NS, (b) Taft EW, (c) Northridge EW, and (d) Kobe NS.

Competing Interests

The authors declare that there is no conflict of interests regarding the publication of this paper.

Acknowledgments

This research was funded by the China National Science Foundation (Project no. 51275369) and National Science and Technology Supporting Program (Project no. 2015BAF06B05). Their supports are gratefully acknowledged.

References

[1] I. H. Mualla and B. Belev, "Performance of steel frames with a new friction damper device under earthquake excitation," *Engineering Structures*, vol. 24, no. 3, pp. 365–371, 2002.

[2] W.-I. Liao, I. Mualla, and C.-H. Loh, "Shaking-table test of a friction-damped frame structure," *Structural Design of Tall and Special Buildings*, vol. 13, no. 1, pp. 45–54, 2004.

[3] J. Kim, H. Choi, and K.-W. Min, "Use of rotational friction dampers to enhance seismic and progressive collapse resisting capacity of structures," *Structural Design of Tall and Special Buildings*, vol. 20, no. 4, pp. 515–537, 2011.

[4] M. Sanati, S. E. Khadem, S. Mirzabagheri, H. Sanati, and M. Y. Khosravieh, "Performance evaluation of a novel rotational damper for structural reinforcement steel frames subjected to lateral excitations," *Earthquake Engineering and Engineering Vibration*, vol. 13, no. 1, pp. 75–84, 2014.

[5] S. Mirzabagheri, M. Sanati, A. A. Aghakouchak, and S. E. Khadem, "Experimental and numerical investigation of rotational friction dampers with multi units in steel frames subjected to lateral excitation," *Archives of Civil and Mechanical Engineering*, vol. 15, no. 2, pp. 479–491, 2015.

[6] M. Mirtaheri, A. P. Zandi, S. S. Samadi, and H. R. Samani, "Numerical and experimental study of hysteretic behavior of cylindrical friction dampers," *Engineering Structures*, vol. 33, no. 12, pp. 3647–3656, 2011.

[7] H. S. Monir and K. Zeynali, "A modified friction damper for diagonal bracing of structures," *Journal of Constructional Steel Research*, vol. 87, pp. 17–30, 2013.

[8] A. Sagirli, C. O. Azeloglu, R. Guclu, and H. Yazici, "Self-tuning fuzzy logic control of crane structures against earthquake induced vibration," *Nonlinear Dynamics*, vol. 64, no. 4, pp. 375–384, 2011.

[9] C. O. Azeloglu, A. Sagirli, H. Yazici, and R. Guclu, "Gantry crane structure seismic control by the use of fuzzy PID cont," *Gazi University Journal of Science*, vol. 26, no. 2, pp. 215–223, 2013.

[10] C. Oktay Azeloglu and A. Sagirli, "Active vibration control of container cranes against earthquake by the use of LMI based mixed H_2H_∞ state-feedback controller," *Shock and Vibration*, vol. 2015, Article ID 589289, 13 pages, 2015.

[11] W. Gong-Xian, W. Yang-Yang, H. Yong, and W. Dong, "Study on seismic response control for a container crane using viscous dampers," *Journal of Vibration and Shock*, vol. 35, no. 12, pp. 171–176, 2016.

[12] J.-D. Kang and H. Tagawa, "Seismic performance of steel structures with seesaw energy dissipation system using fluid viscous dampers," *Engineering Structures*, vol. 56, pp. 431–442, 2013.

[13] J.-D. Kang and H. Tagawa, "Seismic response of steel structures with seesaw systems using viscoelastic dampers," *Earthquake Engineering and Structural Dynamics*, vol. 42, no. 5, pp. 779–794, 2013.

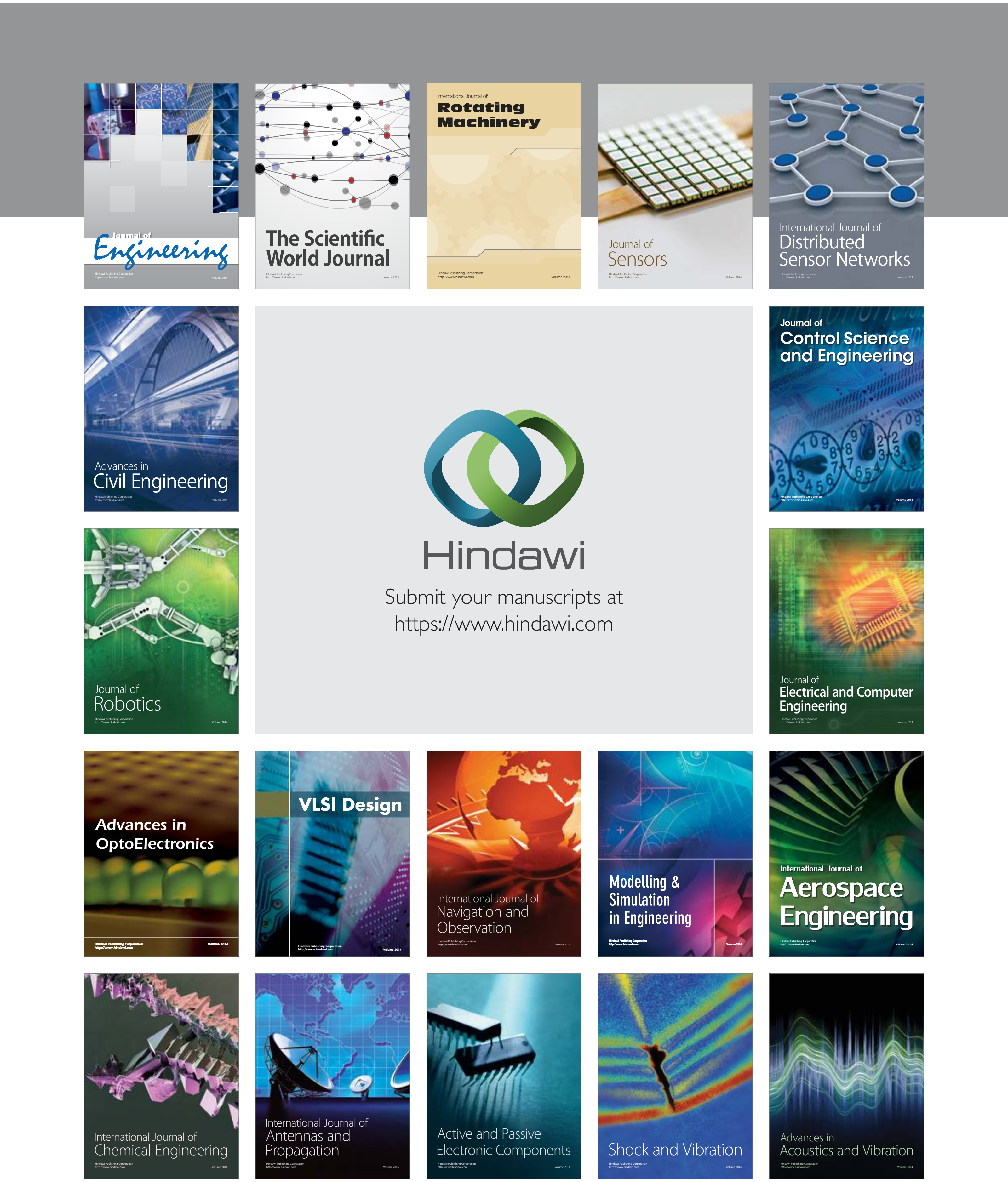
Journal of
Engineering
The Scientific
World Journal
International Journal of
Rotating
Machinery
Journal of
Sensors
International Journal of
Distributed
Sensor Networks
Advances in
Civil Engineering
Hindawi
Submit your manuscripts at
https://www.hindawi.com
Journal of
Control Science
and Engineering
Journal of
Robotics
Journal of
Electrical and Computer
Engineering
Advances in
OptoElectronics
VLSI Design
International Journal of
Navigation and
Observation
Modelling &
Simulation
in Engineering
International Journal of
Aerospace
Engineering
International Journal of
Chemical Engineering
International Journal of
Antennas and
Propagation
Active and Passive
Electronic Components
Shock and Vibration
Advances in
Acoustics and Vibration